J. Fluid Mech. (1982), *vol.* 119, *pp.* 219–247
Printed in Great Britain

Creeping flow in two-dimensional networks

By JOEL KOPLIK

Schlumberger-Doll Research, P.O. Box 307,
Ridgefield, Connecticut 06877, U.S.A.

(Received 20 July 1981)

We discuss creeping incompressible fluid flow in two-dimensional networks consisting of regular lattice arrays of variable-sized channels and junctions. The intended application is to low-Reynolds-number flow in models of porous media. The flow problem is reduced to an analogue linear-network problem and is solved by numerical matrix inversion. It is found that 'effective-medium theory' provides an excellent approximation to flow in such networks. Various qualitative features of such flows are discussed, and an elegant general form for the absolute permeability is derived. The latter, and the effective-medium approximation, are equally applicable to three-dimensional networks.

1. Introduction

The flow of fluids in microscopically disordered porous media is a subject with application to a variety of technological areas, such as hydrology, chemical production processes, and oil recovery (Bear 1972; Collins 1961; Scheidegger 1974). In many cases, one works with an empirically determined Darcy permeability for the porous material in question, but direct measurement is not always practical and does not always provide sufficient information. A broader approach is to calculate the permeability from the microscopic geometry of the medium; one is then in a position to relate changes in microstructure quantitatively to changes in macroscopic variables. A further advantage of calculating from the microscopic level up is that other physical processes may be discussed in parallel, and, by the same token, calculational techniques originally devised to study other transport processes may be brought to bear on the fluid problem.

Our aim in this paper is to calculate approximately the local velocity and pressure fields for creeping flow in a class of network models of porous media. Macroscopic flow parameters, such as the permeability, are obtained by averaging the local flow field. While most of the specific calculations we present refer to certain two-dimensional networks, we shall argue that many of our results are quite general, and that extension to any two- or three-dimensional network involves no new principles.

A typical network that we study is shown in figure 1; it consists of a regular lattice arrangement of junctions or 'pores', connected by channels or 'throats'. The pores and throats are characterized by their radii, with an independent probability distribution function (p.d.f.) for each, and by the centre-to-centre distance. One can consider a pseudo-two-dimensional lattice where the pore separations have a p.d.f. as well. The lattice is further characterized by its co-ordination number σ, the number of throats meeting at a pore; in the figure $\sigma = 4$, and in general σ can be a random variable

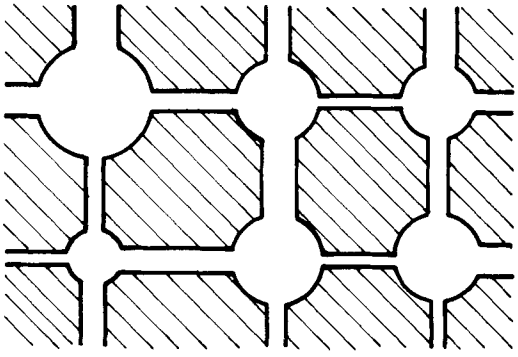

FIGURE 1. Semi-regular network model of a two-dimensional porous medium.

with its own p.d.f. The network approach to porous media is an old one, surveyed by van Brakel (1975), but we are unaware of any previous effort to include the effects of the pores.

To solve the fluid-flow problem, we break up the network into its constituent pores and throats, and match the flow field approximately at the boundaries. We then observe that for each constituent there is a linear relationship between pressure difference and fluid flux, so that the fluid problem maps onto an electrical-resistor problem (Fatt 1956). We then solve the analogue electrical-network problem by inverting the appropriate conductance matrix and averaging over the p.d.f. of the network elements. We find that averaging over the random medium can be carried out semi-analytically using an effective-medium theory.

In many porous media, such as oil reservoir rock, the void space is quite irregular and convoluted, and bears no obvious resemblance to figure 1. Even if one could determine the mathematical function that gives the boundary of the pore space for such a medium, it would be hopeless to attempt any calculation in so irregular a region. Fortunately, there are systematic 'stereological' procedures which convert an irregular pore space into an approximate semi-regular network (Pratt 1978; Serra 1982). For two-dimensional media there already exists computer hardware for this purpose, while the three-dimensional case is an active research area. Obviously, an approach based on the microgeometry of the pore space requires a great deal of input, such as examination of scanning electron micrographs, that is not always readily available. However, one can instead regard the microscopic description of the porous material as a kind of 'basis set' from which one can calculate a variety of physical processes: sound propagation, electric conductivity and dielectric response, nuclear-particle transport, etc. One may then attempt to correlate the different types of physical transport, and deduce the properties of one type from measurements of another. Such empirical correlations are often used in current practice (in the oil-recovery case, the procedure is known as well-logging; see e.g. Pirson (1963)), and further theoretical understanding can only improve matters.

The remainder of this paper is organized as follows. In § 2, we compute the flow field in a pore as a function of the flux entering or leaving the various throats. By matching throat and pore flow only approximately, this calculation can be carried out analytically using complex-variable techniques. We indicate how the matching approximation might be improved upon. Section 3 describes the resistor network

analogy for computing network flows, and reviews effective-medium theory. Some numerical results are presented in § 4; we demonstrate the applicability of the effective-medium approximation using a particular simplified p.d.f., and then study the qualitative features of flow in networks, emphasizing the appearance of Darcy's law and the interplay of pore and throat sizes. The previous results are used in § 5 to express the permeability of networks, in two or three dimensions, in a convenient and suggestive form. In § 6, we summarize our results and indicate future directions.

2. Pore Flow

In this section, we calculate the flow field in the network pores. The basic idea is to divide the network into separate pores and throats, and match pressure and velocity fields where they join. At low Reynolds number, one has Poiseuille flow in the central region of the throats and somewhat different entry and exit flows near the ends, where the lengths of the entry and exit regions are of the order of a throat diameter. Ideally, one should consider a pore with its adjacent entry and exit regions appended, and use as boundary condition a Poiseuille velocity distribution across the throat openings, and zero velocity on the solid boundaries of the pores. This procedure leads to rather irregular pore regions, and requires a numerical calculation. We have instead used a simplifying approximation which yields an analytic solution: we neglect the entry and exit regions, regarding the pores as simple circles, but continue to match to a Poiseuille velocity field in the openings. In consequence, the pressures do not exactly match at the pore–throat boundary. While this simplification is not essential, it is unlikely that the pore-space geometry will be known with high precision in most applications, and we do not think it worthwhile to be very accurate at this point.

The approximated pore flow problem can now be stated as follows (see figure 2*a*). In the two-dimensional region $|\mathbf{x}| \leqslant R$, solve the Stokes equations

$$\mu \nabla^2 \mathbf{u} = \nabla p, \quad \nabla . \mathbf{u} = 0, \tag{1}$$

with the boundary condition on $|\mathbf{x}| = R$ that

$$\mathbf{u} = \begin{cases} \mathbf{u}_{Pi} & (|\theta - \theta_i| \leqslant \arcsin(r_i/R)), \\ \mathbf{0} & \text{(otherwise).} \end{cases} \tag{2}$$

Here, $\mathbf{u}_{Pi}$ is the appropriate Poiseuille flow for throat i; for example

$$\mathbf{u}_{Pi} = \frac{3Q_1}{4r_1^3}(r_1^2 - y^2)\,\hat{\mathbf{x}}, \tag{3}$$

where Q_1 and r_1 are the flux and radius of throat 1. Introducing a stream function $\Psi(\mathbf{x})$ by

$$\mathbf{u} = \left(\frac{\partial \Psi}{\partial y}, \frac{-\partial \Psi}{\partial x}\right), \tag{4}$$

and taking the curl of (1), we have

$$\nabla^4 \Psi = 0, \tag{5}$$

with boundary conditions on $\nabla\Psi$ on $|\mathbf{x}| = R$.

We can solve the biharmonic equation for this case in closed form by a complex-

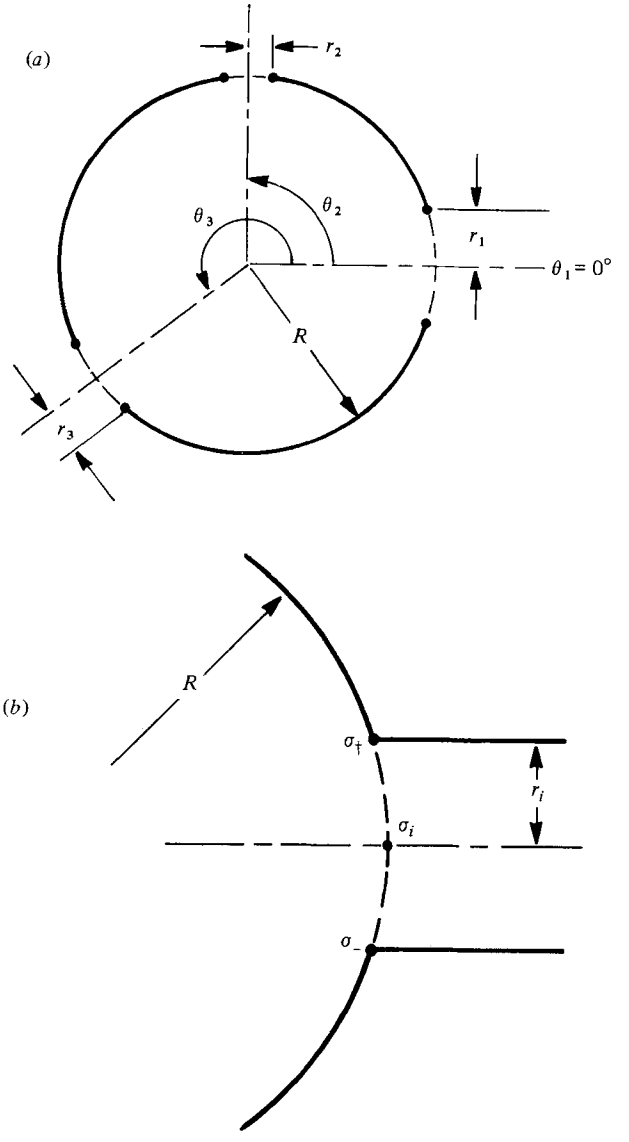

FIGURE 2. (*a*) Geometry of a pore. (*b*) Detailed geometry near a pore exit.

variable technique due to Muskhelishvili (1953);† see also Kantorovich & Krilov (1958). Introducing complex co-ordinates

$$z = \frac{x+iy}{R}, \quad \bar{z} = \frac{x-iy}{R}, \tag{6}$$

the biharmonic equation (5) becomes

$$\left(\frac{\partial^2}{\partial z\,\partial\bar{z}}\right)^2 \Psi(z,\bar{z}) = 0. \tag{7}$$

† Alternatively one could use Fourier-series methods, as in Mills (1977). I thank a referee for bringing this reference to my attention.

A general solution of (7) is a linear function of $\bar{z}$, which we write in the form

$$\Psi = -\mathscr{R}[\phi(z)+\bar{z}\chi(z)]. \tag{8}$$

In terms of the analytic functions ϕ and χ, the velocity is

$$V \equiv v-iu = \phi(z)+z\overline{\phi'(z)}+\overline{\chi'(z)}, \tag{9}$$

and the pressure is (Langlois 1964)

$$p(z) = p(0)+4\mu\mathscr{I}\phi'(z). \tag{10}$$

The problem is now to find ϕ and χ such that, on $|z| = 1$, V takes the value

$$V_0(\theta) = \begin{cases} -\dfrac{3iR^2Q_j}{4r_j^3}e^{i\theta_j}\left[\left(\dfrac{r_j}{R}\right)^2-\sin^2(\theta-\theta_j)\right] & (|\theta-\theta_j| \leqslant \arcsin(r_j/R)), \\ 0 \quad \text{(otherwise)}. \end{cases} \tag{11}$$

We will proceed by integrating (9) around the unit circle; on $|z| = 1$ we write

$$z = \sigma = e^{i\theta},$$

so (9) and its complex conjugate are

$$\left.\begin{aligned} \phi(\sigma)+\sigma\overline{\phi'(\sigma)}+\overline{\chi'(\sigma)} &= V_0(\sigma), \\ \overline{\phi(\sigma)}+\frac{1}{\sigma}\phi'(\sigma)+\chi'(\sigma) &= \overline{V_0(\sigma)}. \end{aligned}\right\} \tag{12}$$

We need the following identities, which are valid for $|z| < 1$ and $f(z)$ analytic in $|z| \leqslant 1$:

$$\int_{|\sigma|=1}\frac{d\sigma}{2\pi i}\times\begin{Bmatrix} \dfrac{f(\sigma)}{\sigma-z} \\ \dfrac{\overline{f(\sigma)}}{\sigma-z} \\ \dfrac{\overline{\sigma f(\sigma)}}{\sigma-z} \\ \dfrac{f(\sigma)}{\sigma(\sigma-z)} \end{Bmatrix} = \begin{Bmatrix} f(z), \\ \overline{f(0)}, \\ z\overline{f(0)}+\overline{f'(0)}, \\ \dfrac{1}{z}[f(z)-f(0)]. \end{Bmatrix} \tag{13}$$

The first identity is Cauchy's theorem, while the others are easily derived from the Taylor-series expansions of $f(z)$ and $(1-z/\sigma)^{-1}$ by termwise integration. Now integrating (12) around the unit circle and making use of (13), we obtain

$$\left.\begin{aligned} \phi(z)+z\overline{\phi'(0)}+\overline{\phi''(0)}+\overline{\chi'(0)} &= \int_{|\sigma|=1}\frac{d\sigma}{2\pi i}\frac{V_0(\sigma)}{\sigma-z}, \\ \overline{\phi(0)}+\frac{\phi'(z)-\phi'(0)}{z}+\chi'(z) &= \int_{|\sigma|=1}\frac{d\sigma}{2\pi i}\frac{\overline{V_0(\sigma)}}{\sigma-z}. \end{aligned}\right\} \tag{14}$$

The constants $\phi'(0)$, $\phi''(0)$ and $\chi'(0)$ may be obtained from the low-order Fourier coefficients of V_0. We expand

$$V_0(\sigma) = \sum_{n=-\infty}^{\infty} a_n e^{in\sigma}, \tag{15}$$

and insert the Taylor-series expansions for ϕ and χ into (12), taking advantage of the arbitrariness in the definition (4) to set $\phi(0) = 0$. Comparing powers of σ, we find

$$\phi'(0) = \tfrac{1}{2}a_1, \quad \phi''(0) = 2a_2, \quad \chi'(0) = a_0 - 2a_2. \tag{16}$$

It is in fact possible to solve for ϕ and χ term by term by this procedure, providing an independent derivation of (14).

In the equations (14), the right-hand side is known from $V_0(\sigma)$, the constants are given in terms of V_0 by (15) and (16), so the first equation gives $\phi(z)$, the second then gives $\chi'(z)$, and the problem is solved. ($\chi(0)$ is undetermined and irrelevant.) If the pore has a more-complicated shape that can be conformally mapped into a circle, then Muskhelishvili's method gives ϕ and χ as the solution of a coupled pair of Fredholm integral equations.

In practice, the explicit solution obtained by inserting (11) into (14) is fairly complicated:

$$\phi(z) = \sum_i \frac{3iQ_i e^{i\theta_i}}{8\pi a_i^3}\left[(2a_i^2 - 1)\arcsin a_i + a_i(1-a_i^2)^{\frac{1}{2}} + \frac{i}{4}I_i(ze^{-i\theta_i})\right], \tag{17}$$

where the sum runs over entries and exits i, $a_i = r_i/R$, and

$$I_i(w) = (4a_i^2 - 2 + w^2 + w^{-2})\log\left(\frac{e^{+i\theta_i} - w}{e^{-i\theta_i} - w}\right) - \frac{2i}{w^2}\arcsin a_i + 2ia_i\left((1-a_i^2)^{\frac{1}{2}} + w - \frac{1}{w}\right), \tag{18}$$

and $\chi'(z)$ is given by a similar expression. Several qualitative features of this solution may be noted.

Superposition. ϕ and χ receive independent, additive contributions from all parts of the unit circle. Given two flows, each with its set of entry and exit throats and each conserving mass, one can contact a new flow field by adding ϕ and χ (or $\mathbf{u}$ and p) locally. In particular, any flow may be regarded as a sum of 'two-port' flows, each with one entry and one exit throat. These statements are exact only when we neglect entry and exit regions for the throats, but should hold approximately in general.

Linearity. From (17) we can represent the potentials schematically as a sum over contributions from each port:

$$\phi(z), \chi'(z) \sim \sum_i Q_i F_i(z). \tag{19}$$

We have extracted the flux Q_i, so the remaining factor $F_i(z)$ depends purely on the geometry of the pore. The pressure and velocity fields are linear in ϕ and χ and have a similar schematic representation. The relative pressure at the centre of port j,

$$p_j \equiv p(z = e^{i\theta_j}) - p(0), \tag{20}$$

has from (10) and (19) the form

$$p_j = \sum_i W_{jk} Q_k. \tag{21}$$

The W_{jk} above are obtained by manipulation and evaluation of the previous expressions and have the form of viscosity times a function of pore and throat geometry (see below). The form (21) is a general consequence of the Stokes equations and the 'factorization' of the flows in separate pores induced by the connecting throats, and is valid for pores of any shape and dimension.

Qualitative z dependence. The functions $F_i(z)$ in (19) are of the form

$$F_i(z) \sim \int_{\sigma_-}^{\sigma_+} d\sigma \frac{V_0(\sigma)}{\sigma - z} = \frac{1}{\sigma_i - z} \int_{\sigma_-}^{\sigma_+} d\sigma\, V_0(\sigma) \left(1 + \frac{\sigma - \sigma_i}{z - \sigma_i} + \ldots\right) \tag{22}$$

(see figure 2*b*), so each F_i tends to decrease with distance from its respective port i. For the pressure we have

$$p(z) \sim \phi'(z) \sim \sum_i Q_i \left(\frac{c_i}{(\sigma_i - z)^2} + \ldots\right), \tag{23}$$

each term of which decreases *rapidly* away from its respective port. Hence for p_j, the relative pressure at the centre of port j, the dominant contribution comes from that term corresponding to port j itself, and (21) simplifies to

$$p_j \simeq W_{jj} Q_j. \tag{24a}$$

Using the explicit expressions above to evaluate W_{jj}, we find

$$p_j \simeq \frac{3\mu}{2\pi a_j^3 R^2} \left[a_j + \arcsin a_j + \frac{a_j^2 \arcsin a_j}{1 - (1 - a_j^2)^{\frac{1}{2}}}\right] Q_j, \tag{24b}$$

(recall $a_j = r_j/R$). By comparison with the direct numerical evaluation of (17) and (18) we find that (24) is accurate to at worst a few per cent when the throats are well-separated. The greatest discrepancy occurs for a pore with two diametrically opposite ports of $a_j = 1$ – a section of straight channel – where (24) overestimates the pressure difference by a multiplicative factor $1 + 1/\pi$. The complete expression (21) is, however, exact in this limit.

The approximate expression (24*b*) may be simplified further by observing (numerically) that the quantity in brackets is approximately equal to $4a_j$, to an accuracy of a few per cent, over the entire range of a. We then have

$$p_j \simeq \frac{6\mu}{\pi r_j^2} Q_j, \tag{24c}$$

an expression independent of the pore radius R. Thus the pressure drop between port j and the centre of the pore is approximately the same as the pressure drop over an additional length $4r_j/\pi$ of throat.

Singularities. By construction, the velocity is continuous across the curve $|z| = 1$ where pore and throat join. However, in figure 2(*b*), for example, the velocity is entirely along the x-axis in the throat to the right, but has both x- and y-components in the pore to the left. The velocity gradients then have jump discontinuities across $|z| = 1$, and the Stokes equation implies that the pressure will have a discontinuity as well. As the corner is approached, a logarithmic singularity develops. Using the schematic form (22), as $z \to \sigma_+$ (the upper corner) the part of the integral near σ_+ dominates; V_0 vanishes linearly there because the corner is part of the solid boundary of the void space, so

$$\phi(z) \underset{z \to \sigma_+}{\longrightarrow} \int^{\sigma_+} d\sigma \frac{\sigma - \sigma_+}{\sigma - z} + \text{regular} = (z - \sigma_+) \log (z - \sigma_+) + \text{regular}. \tag{25}$$

$\phi(z)$ is thus finite at σ_+, but $p \sim \mathscr{R}\phi'(z)$, so

$$p(z) \underset{z \to \sigma_+}{\longrightarrow} \log (z - \sigma_+) + \text{regular}. \tag{26}$$

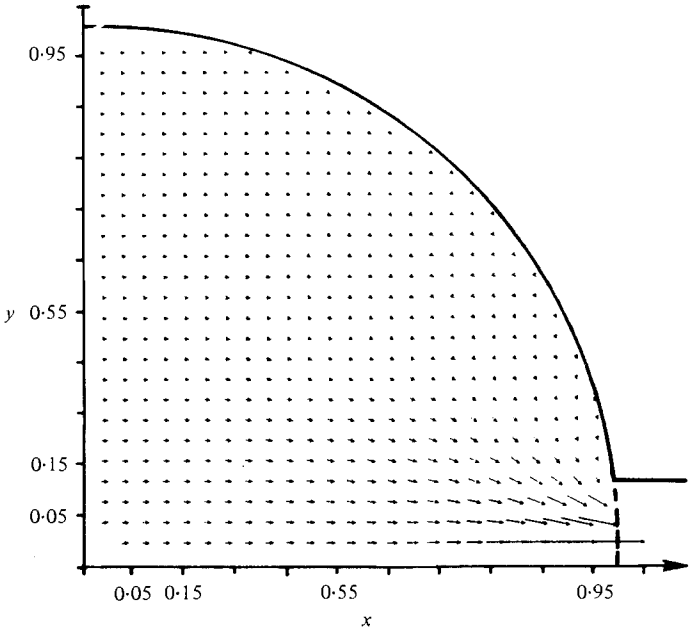

FIGURE 3. Computed interior velocity field in the first quadrant for flow in a pore with two opposite ports of radii $r/R = 0{\cdot}1$.

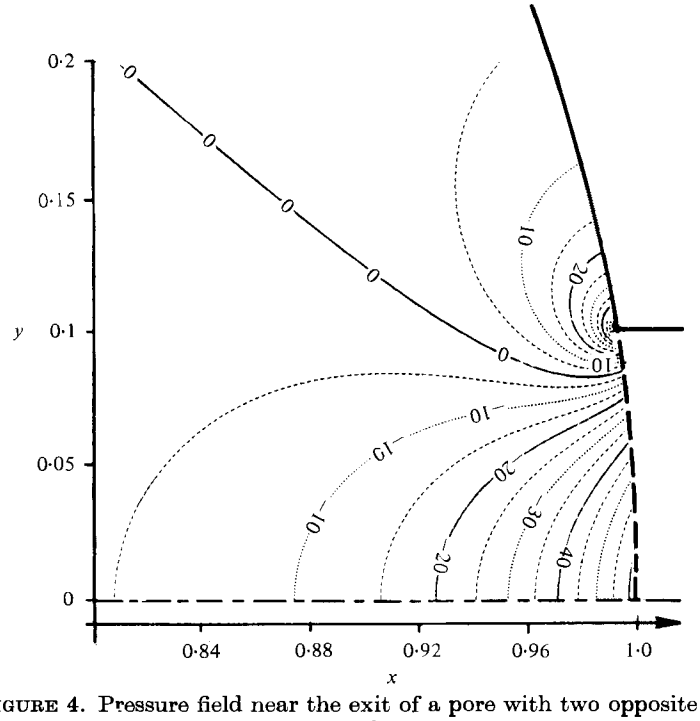

FIGURE 4. Pressure field near the exit of a pore with two opposite ports of radii $r/R = 0{\cdot}1$.

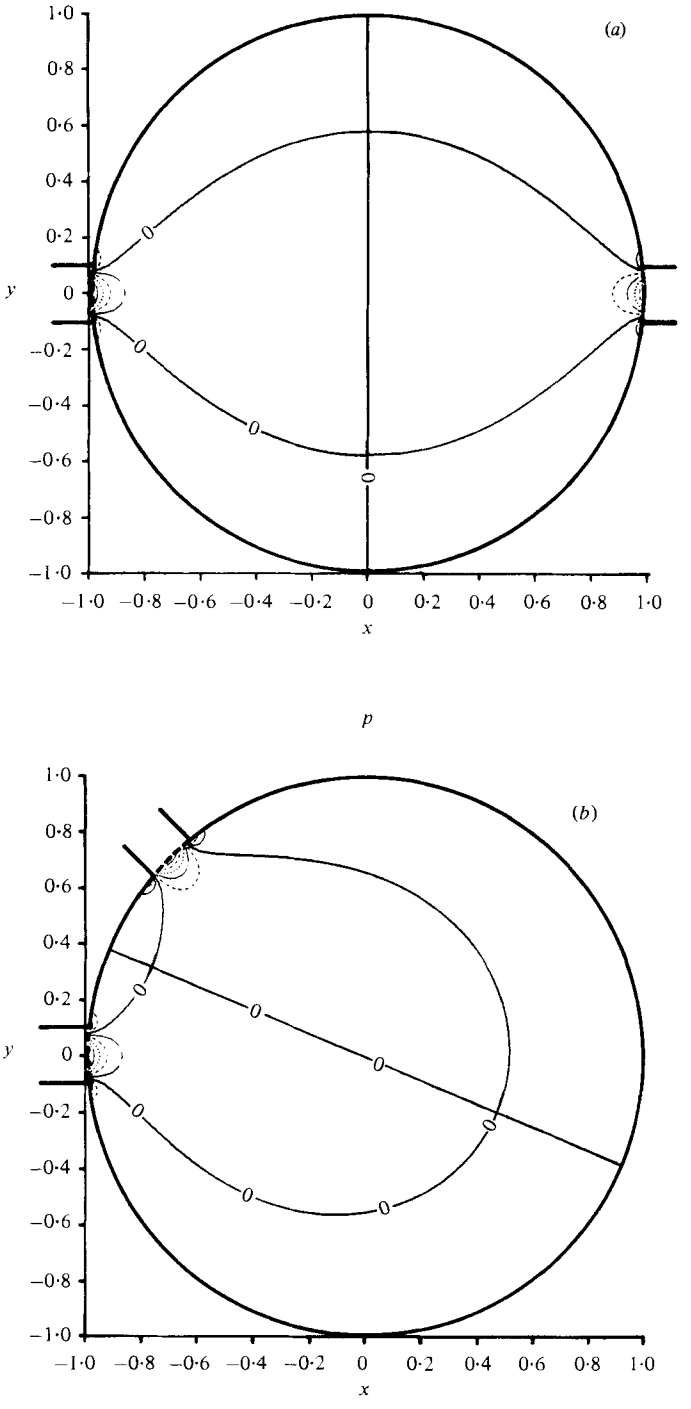

FIGURE 5. The pressure field in a pore with two ports of radius $r/R = 0{\cdot}1$ and entrance at 180°, with the exit at (*a*) 0° and (*b*) 135°.

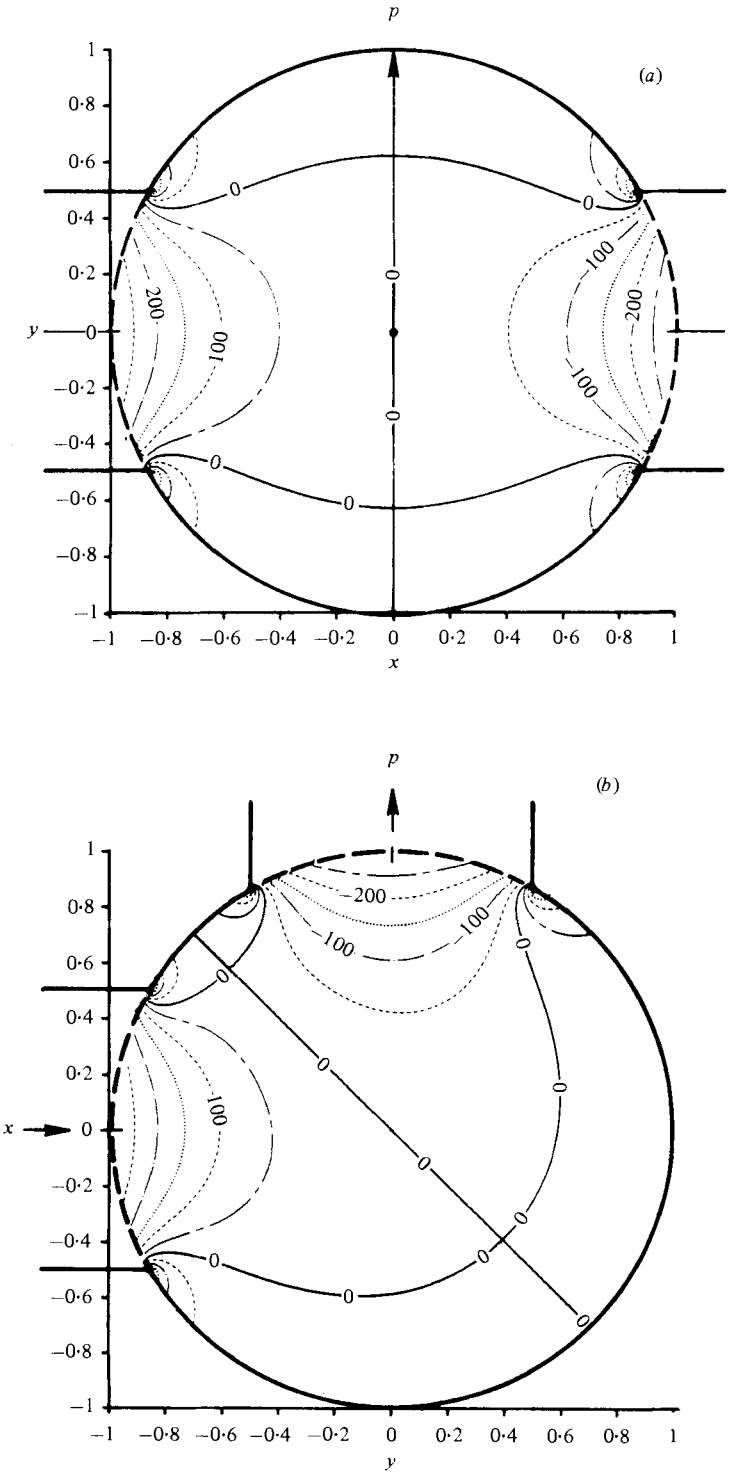

FIGURE 6. Pressure field in a pore with two ports of radius $r/R = 0{\cdot}5$, with the exit at (*a*) 0°, and (*b*) 90°.

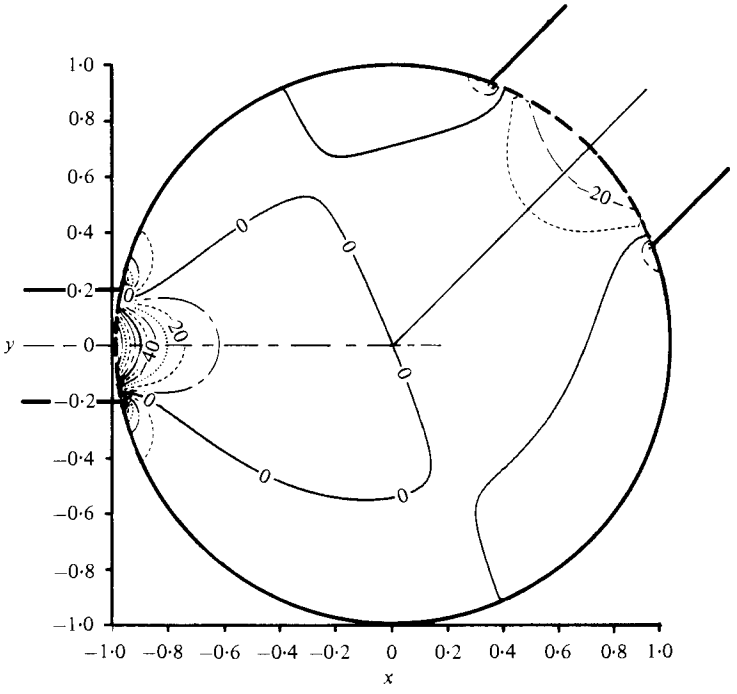

FIGURE 7. A pore with an entry port of relative radius $r/R = 0{\cdot}2$ at 180°, and an exit of radius 0·4 oriented at 45°.

If the sharp corner at σ_+ were rounded off, then $V_0(\sigma)$ would vanish quadratically there and $p(\sigma_+)$ would be finite. Had we matched pores and throats more accurately, a power singularity would be expected at a sharp corner (Moffatt 1964).

Finally, we display some examples of the resulting p and $\mathbf{u}$ fields inside a pore. In figures 3 and 4, we consider a pore of unit radius with an entry port at $\theta_1 = 180°$ and an exit port at $\theta_2 = 0°$, both with $r/R = 0{\cdot}1$. The velocity field in the first quadrant is shown in figure 3, where the orientation and length of the arrows give the direction and relative magnitude of $\mathbf{u}$ at evenly spaced grid points. The pressure field near the exit is shown in figure 4; the units are arbitrary, with $p = 0$ at the origin and $p = -63{\cdot}5$ at the centre of the exit. The fields in the other quadrants follow by symmetry. Note that, as argued qualitatively above, the pressure is approximately zero outside the exit (and entry) regions. To emphasize this point, as well as to indicate the independence of different ports, in figure 5 we show the full pressure field in the full unit circle as the orientation of the exit port varies from 0° (figure 5*a*) to 135° (figure 5*b*). As the radii of the ports increase, the region over which the pressure field is appreciably non-zero extends further into the pore's interior. In figure 6, we consider ports of radius 0·5 with an entry at 180° and exits first at 0° (figure 6*a*), and then at 90° (figure 6*b*). Lastly, we display in figure 7 the pressure field for an unsymmetric example, with an entry port of radius 0·2 at 180° and an exit port of radius 0·4 at 45°.

In the remainder of this paper we match the flow fields at the pore–throat boundary by identifying the pressures at the centre of the boundary line, using (20) as the definition of the pressure drop across a pore. Our rationale for this choice is that the

flow along the centre line of the throat would be at least affected by an improved matching procedure.

3. Analogue resistor network

In the flow network of figure 1, consider any two neighbouring pores a and b, and their connecting throat. The pressure difference between the two pore centres is the sum of two pore-pressure differences and a throat-pressure difference:

$$\Delta p_{ab} = p_a + p_t + p_b.$$

Using the approximation (23) for the pores and the (two-dimensional) Poiseuille result for the throat

$$p_t = \frac{3\mu l}{2r^3} Q_{ab}, \tag{27}$$

we can write

$$\Delta p_{ab} = \left(W_{aa} + \frac{3\mu l}{2r^3} + W_{bb}\right) Q_{ab} \equiv g_{ab}^{-1} Q_{ab} \tag{28}$$

Furthermore, the fluid is incompressible and flux is conserved at each pore:

$$\sum_{a \to b} Q_{ab} = 0, \tag{29}$$

where the sum is over all pores a connected directly to b. The two equations (28) and (29) are formally identical to the equations of an electrical-resistor network (Fatt 1956; Dullien 1979) with the correspondence

$$\left.\begin{aligned} \text{pressure} &\Leftrightarrow \text{voltage}, \\ \text{fluid flux} &\Leftrightarrow \text{electric current}, \\ g_{ab} &\Leftrightarrow \text{electrical conductance}, \end{aligned}\right\} \tag{30}$$

and we may solve them by the same methods. Inserting (28) into (29), we have

$$\sum_{a \to b} g_{ab}(p_a - p_b) + S_b = 0, \tag{31}$$

where we have allowed for a possible external fluid source S_b. In practice, S_b will be non-zero only at the boundaries of the network. The last equation may be rearranged in matrix form as

$$\mathbf{G} \cdot \mathbf{P} = \mathbf{S}, \tag{32}$$

where $\mathbf{P} = (p_1, p_2, \ldots, p_N)^{\mathrm{T}}$ is a vector of pore (-centre) pressures, similarly for $\mathbf{S}$, and the 'conductance matrix' $\mathbf{G}$ is

$$G_{ab} = \delta_{ab}\left(\sum_{c \to a} g_{ca}\right) - g_{ab}. \tag{33}$$

Had we retained the more-general form (21) for the pore pressures, we would still obtain (32) but with a more complicated conductance matrix involving neighbouring throats.

The problem is now to invert the conductance matrix $\mathbf{G}$. We are particularly interested in the case where internal pore and throat dimensions vary according to some probability distributions, so it will be necessary to repeat the inversion with different

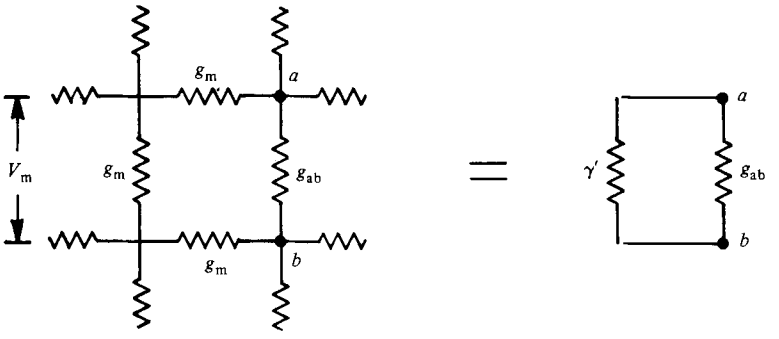

FIGURE 8. Determining the EMT conductance.

realizations of the probability distribution, and then average. Some numerical results appear in § 4.

A common approximation in the physics of microscopically disordered media is 'effective-medium theory' (EMT), in which one seeks to replace random microscopic parameters with a certain mean value, chosen so that the mean field produced by the random parameters is the same as that produced when all parameters have this mean value. Approximations of this sort have been applied with considerable success to a variety of problems in solid-state physics (see e.g. Ziman 1979), and a version of EMT appropriate to random networks has been given by Kirkpatrick (1973). We shall see in § 4 that network EMT does quite well, so we digress here to review Kirkpatrick's derivation. We shall use electrical terminology, but with the correspondence (30) similar statements apply for fluid networks.

Suppose we have an infinite resistor network of co-ordination number σ, with individual bond conductances g_{ab}, and we wish to choose a mean EMT conductance g_m in such a way that the mean conductances reproduce the average local field. If in the EMT network one conductance reverts from g_m back to its original value g_{ab}, there will be an excess current in that resistor of

$$\Delta I = (g_m - g_{ab}) V_m,$$

where V_m is the potential difference between nodes in the mean network (see figure 8). The excess current produces an excess voltage

$$\Delta V_{ab} = \frac{\Delta I}{g_{ab} + \gamma'_{ab}},$$

where γ'_{ab} is the conductance of the rest of the network between the end points of g_{ab}. To find γ'_{ab}, observe that, if g_{ab} were replaced by g_m, then g_m and γ'_{ab} in parallel would give the node-to-node conductance γ_{ab} of the EMT network:

$$\gamma_{ab} = \gamma'_{ab} + g_m.$$

γ_{ab} is relatively easy to calculate: by definition of node-to-node conductance, if current I enters node a and leaves node b producing potential difference V_{ab}, then $\gamma_{ab} = I/V_{ab}$. However, this situation is the linear superposition of current I entering node a and leaking out at infinity, and current I leaking in at infinity and exiting node b. In the former case, current I/σ is present in all resistors leading out of a, including ab, so

$V_{ab} = I/\sigma g_m$. In the latter case, the same current and the same voltage drop occur in ab, so adding we have

$$V_{ab} = \frac{1}{g_m}\frac{2I}{\sigma}.$$

This gives γ_{ab}, which gives γ'_{ab}, which gives

$$\Delta V_{ab} = V_m \frac{g_m - g_{ab}}{g_{ab} + (\frac{1}{2}\sigma - 1)g_m}.$$

The value of g_{ab} and hence of ΔV_{ab} is a random variable, and we require that the average of ΔV_{ab} with respect to the probability distribution $p(g_{ab})$ vanish:

$$\left\langle \frac{g_m - g}{g + (\frac{1}{2}\sigma - 1)g_m} \right\rangle_{p(g)} = 0. \tag{34}$$

The EMT conductance g_m is chosen so that (34) is satisfied.

It is easy to show from (34) that $g_m(\sigma)$ is a monotonically increasing function of σ, with the property

$$g_m(2) = \langle g^{-1}\rangle^{-1} \leqslant g_m(\sigma) \leqslant \langle g\rangle = g_m(\infty).$$

The lower bound on $g_m(\sigma)$ corresponds to conductors in series, while the upper bound corresponds to conductors in parallel, and the inequality states that an interconnected network is somewhere in between.

The argument just given does not make explicit the circumstances under which the EMT approximation should be valid. We have studied this question in detail in another publication (Koplik 1981), for the case of completely uncorrelated local conductances. We find that the essential requirement for EMT to perform well is that the conductance probability distribution be 'non-critical', not strongly weighted near $g = 0$ and, more specifically, that the system not be near the conduction threshold. When this condiction is not met, one may instead take direct advantage of the fact that the system is near a critical point and make use of scaling relations, the renormalization group, and other methods used for phase transitions. While we do not pursue this case further here, discussions of the analogous electrical-conductivity problem are given by Kirkpatrick (1973) and articles by Kirkpatrick, Lubensky, and Thouless in Balian, Maynard & Toulouse (1979).

4. Numerical results

4.1. *Procedure*

We solve the network equations (32) and (33) numerically by the following method. A flow configuration is chosen, usually that shown in figure 9 where we assign pressure p_L to all nodes on the left boundary of the network, pressure $p_R < p_L$ on the right boundary, and periodic boundary conditions on the remaining sides, so the average flow is from left to right. With this choice, the source vector **S** has the form

$$S_a = \begin{cases} g_{La}\, p_L & (a \in \text{left boundary}), \\ g_{Ra}\, p_R & (a \in \text{right boundary}), \\ 0 & (\text{otherwise}), \end{cases} \tag{35}$$

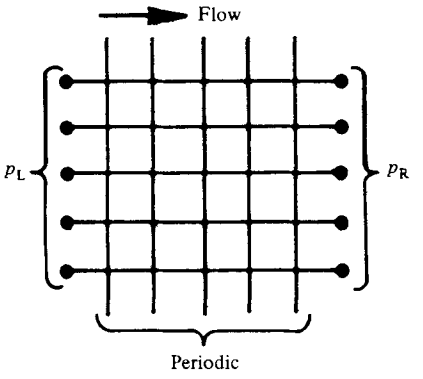

FIGURE 9. Standard flow configuration for determining network conductances.

where the random conductances g_{La} and g_{Ra} appear in the appropriate diagonal elements of **G** as well. Normally one chooses periodic boundary conditions to minimize finite-sample-size effects, but we shall see that no-flow boundary conditions on the sides give virtually identical results.

A set of pore and throat radii and throat lengths are chosen according to their respective probability distributions, the conductances g_{ab} are computed, and the conductance matrix **G** is constructed. Equation (32) is solved for **P**, using a commercially available linear-algebra package, and the total flux Q is computed as

$$Q = \sum_a (p_L - p_a)\, g_{La}. \tag{36}$$

The sum in (36) runs over the left boundary of the network. The procedure is repeated with a new set of throat radii, etc., and we compute average pore pressures $\langle \mathbf{P} \rangle$ and an average total fluid flux $\langle Q \rangle$.

4.2. *Comparison with effective-medium theory*

In this and the following subsection, we study those features of network flow that depend only on the conductances g_{ab} having a probability distribution, postponing the comparison of different distributions to § 4.3. We have arbitrarily selected the uniform conductance distribution

$$p(g_{ab}) = \begin{cases} \frac{1}{4999} & (1 \leqslant g_{ab} \leqslant 5000), \\ 0 & (\text{otherwise}) \end{cases} \tag{37}$$

as illustrative of broad distributions. It is intuitively reasonable that any peaked distribution with the same endpoints or any narrower uniform distribution can only improve the accuracy of an averaging procedure, while in another publication (Koplik 1981) we show that any broadening of the distribution will not alter our conclusions. It is essential, however, that the conductance distribution not correspond to a system near the conduction threshold ($p(g_{ab})$ largest near $g_{ab} = 0$), where mean-field approximations are invalid. In figure 10, we show the various lattices we have studied numerically. Note that, aside from variation in co-ordination number, we have allowed for variation in spatial dimension (trigonal *vs.* cubic), and in topology beyond co-ordination number (square *vs.* Kagomé).

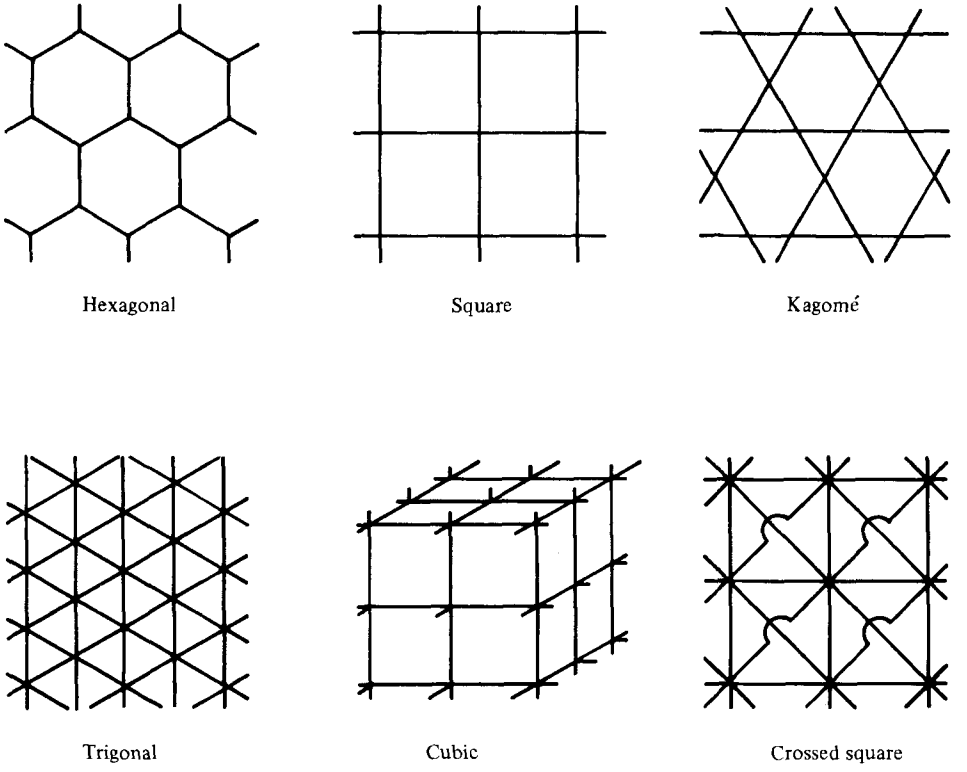

FIGURE 10. Lattices studied in this work.

The comparison of numerical results with EMT is simplest in terms of an 'effective conductance', g_{eff}. We first compute an overall network conductance

$$K = \frac{\langle Q \rangle}{p_{\text{L}} - p_{\text{R}}}, \tag{38}$$

which is related to the permeability of the network by factors depending on the overall geometry, but not the details of the conductance distribution (see § 5). We then compute K with all conductances set to one, and define

$$g_{\text{eff}} = \frac{K(\{g_{ab}\})}{K(\{1\})}. \tag{39}$$

If all internal conductances were set equal to g_{eff} the network conductance $K(\{g_{ab}\})$ would be reproduced, and to the extent that EMT is valid we expect $g_{\text{eff}} = g_{\text{m}}$. In table 1, we compare g_{eff} with g_{m} for the various lattices studied, where in all cases we have averaged over 100 runs on a lattice of the order of 100 pores. The agreement is well within the statistical standard deviation in each case, and the variation of the mean numerical value is just as expected from EMT. Beyond this 'global agreement', we shall see presently that EMT provides an excellent approximation even to average individual pore pressures.

The last column in table 1 gives the effective conductance of networks where the co-ordination number does not have a precise value but a probability distribution. We

Lattice	$g_m(\sigma)$	$g_{eff}(\sigma)$	$g_{eff}(\langle\sigma\rangle)$
Hexagonal	1752	1786 ± 187	1862 ± 205
Kagomé	1991	2000 ± 189	—
Square	1991	2002 ± 147	2044 ± 146
Trigonal	2186	2206 ± 130	2212 ± 145
Cubic	2186	2182 ± 99	—
Crossed square	2272	2280 ± 83	—

TABLE 1. Comparison of EMT conductances g_m to numerical average conductances g_{eff} for various lattices, with conductance p.d.f. (37)

begin with the $\sigma = 8$ crossed-square network shown in figure 10, and randomly set throat radii to zero with probability $(1 - \frac{1}{8}\langle\sigma\rangle)$. The probability of k throats remaining open is then

$$\binom{8}{k} (\tfrac{1}{8}\langle\sigma\rangle)^k (1 - \tfrac{1}{8}\langle\sigma\rangle)^{8-k},$$

1, we have a binomial distribution with mean $\langle\sigma\rangle$. For the cases studied in table $g_{eff}(\langle\sigma\rangle) \simeq g_m(\langle\sigma\rangle)$. In microscopically disordered porous media, there is likely to be a distribution of co-ordination numbers rather than a single fixed value, so this result is of some practical importance.

4.3. *Qualitative flow features*

In figures 11–13, we display the variation of network conductance K with network size, for a square $\sigma = 4$ lattice. To the extent that the random conductances are well represented by a single effective conductance, we expect

$$K = g_{eff} \frac{N_\perp}{N_\parallel} \quad (\sigma = 4), \tag{40}$$

where $N_\parallel$ and $N_\perp$ are the number of lattice links along and orthogonal to the flow direction, respectively, and from the results of § 4.2 $g_{eff} \simeq g_m$. The numerical results in figures 11 and 12 give a length and width dependence quite in accord with (40), even for surprisingly small lattices. More generally, for overall-square networks ($N_\parallel = N_\perp = N$), figure 13 shows no significant size dependence once $N > 3$. The second set of points in figure 13 are the analogous results for networks with a no-flow boundary condition on the sides; for $N > 6$ there is no systematic difference between no-flow and periodic boundaries. Similar results are obtained for the other lattices in figure 10. We conclude that averaging of a random conductance distribution – replacing random local conductances by a single (EMT) average value – is valid to an accuracy of order 1 % when the network's linear dimensions exceed several lattice units.

In the same vein, we show in figure 14 the variation of average pressure with distance along the flow for an $N = 10$ square lattice. The pressure is a linearly decreasing function of distance in the flow direction, as it must be if EMT averaging is valid. This result is a kind of demonstration of Darcy's law: to the extent that one can divide the pore space of a porous medium into connected microscopic units in each of which pressure difference is proportional to flux as in (28), the validity of EMT ensures a linear constant average pressure gradient and a linear proportionality between overall pressure difference and total fluid flux.

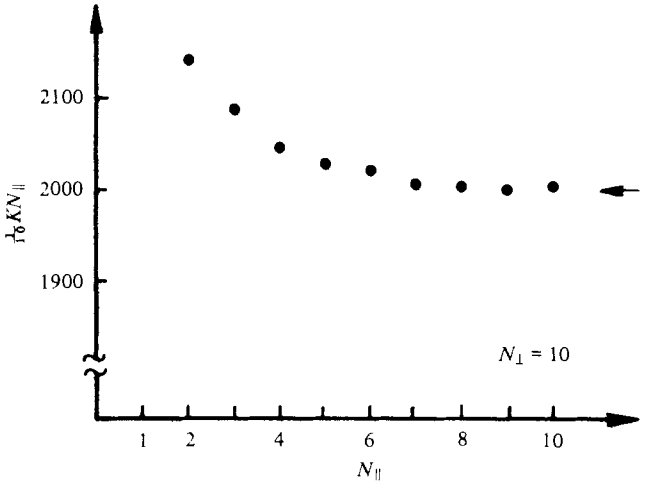

FIGURE 11. Length dependence of the network conductance. The arrow indicates the effective-medium value.

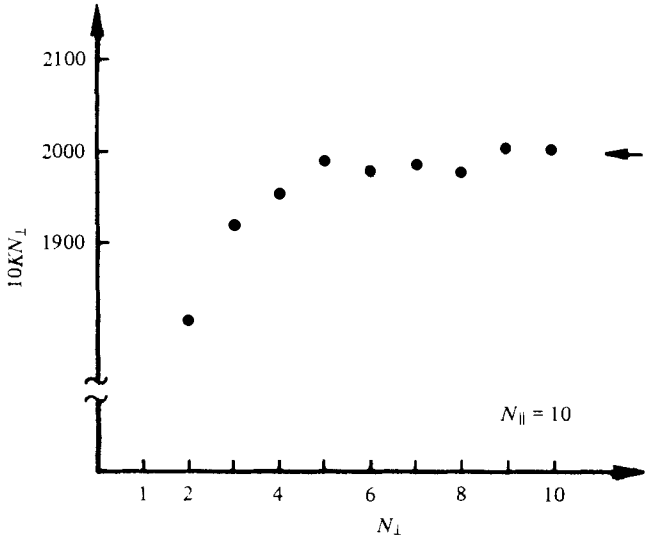

FIGURE 12. Width dependence of the network conductance.

In figure 15, we display the average pore pressures for an irregular flow geometry. The figure shows a square 10×10 lattice with fluid entering one pore on the left from a reservoir at pressure 100 and exiting one (displaced) pore on the right into a reservoir at pressure 0. The pore pressures averaged over 100 runs for this flow configuration, together with the corresponding pore pressures obtained by using g_m everywhere, are given in table 2. (The numbers in table 2 are to be associated with the nodes in figure 15.) The agreement is well within the statistical errors, which are *ca.* 5 %. An interesting feature of this flow configuration is the insensitivity of the network conductance to the precise location of the exit pore: as the position of the exit pore varies all along the right boundary of the lattice, the variation in K is at most 1 %. (In terms of our electrical analogy (30), this behaviour explains why electrical appliances

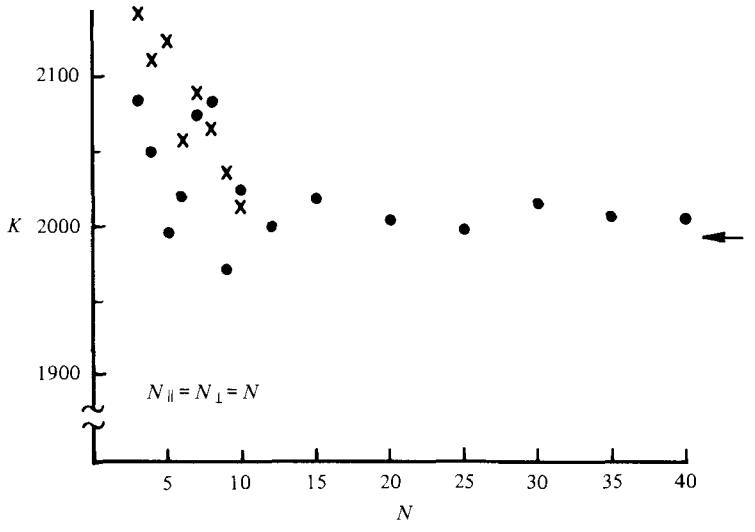

FIGURE 13. Overall-size dependence of the network conductance. The dots and crosses refer respectively to periodic and impermeable side boundaries.

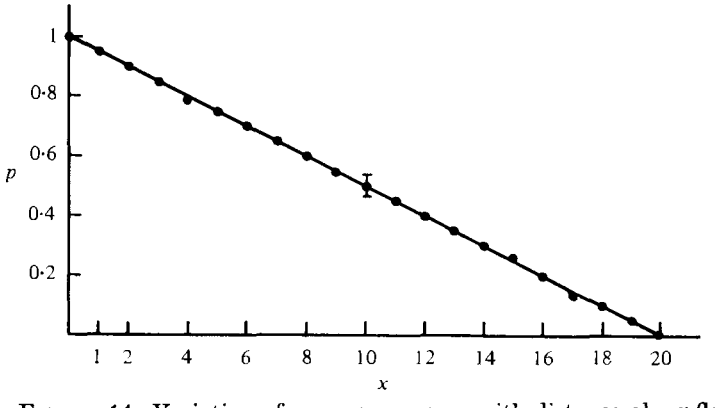

FIGURE 14. Variation of average pressure with distance along flow.

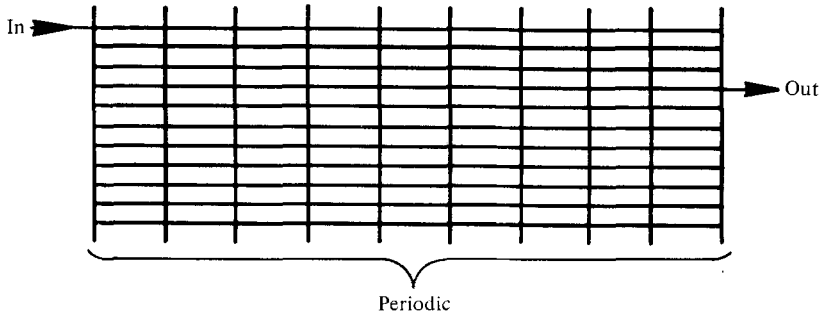

FIGURE 15. Unsymmetric flow configuration.

(*a*)	100	74·99	64·60	59·43	55·64	52·66	49·75	47·29	44·82	42·57	40·63	39·37	
		66·58	62·27	58·58	55·26	52·59	49·55	46·93	44·18	41·29	38·87	37·05	
		61·70	59·93	57·33	54·70	52·06	49·30	46·60	43·31	40·07	36·36	32·69	
		59·21	58·14	56·29	54·02	51·59	49·06	46·35	43·30	38·96	33·91	25·01	0
		57·98	57·15	55·60	53·62	51·49	49·13	46·37	43·28	39·96	36·24	32·52	
		57·55	56·76	55·39	53·56	51·47	49·28	46·64	43·86	41·37	38·89	37·35	
		57·92	57·07	55·69	53·76	51·63	49·43	47·03	44·56	42·37	40·58	39·62	
		59·13	58·11	56·42	54·29	52·01	49·54	47·30	45·11	43·14	41·69	40·99	
		61·50	59·89	57·58	54·90	52·31	49·79	47·47	45·27	43·36	42·02	41·31	
		65·70	62·42	58·64	55·46	52·71	49·86	47·54	45·19	43·12	41·63	40·86	
(*b*)	100	74·50	64·98	59·86	56·22	53·17	50·40	47·80	45·35	43·11	41·26	40·12	
		66·51	62·75	59·10	55·88	52·94	50·16	47·44	44·75	42·08	39·58	37·73	
		62·27	60·42	57·92	55·25	52·56	49·84	47·06	44·12	40·90	37·25	33·49	
		59·88	58·74	56·89	54·65	52·20	49·60	46·83	43·78	40·14	35·02	25·50	0
		58·64	57·77	56·24	54·26	52·00	49·53	46·89	44·02	40·84	37·22	33·47	
		58·26	57·47	56·04	54·17	51·99	49·64	47·16	44·59	42·00	39·53	37·69	
		58·66	57·80	56·30	54·36	52·18	49·86	47·51	44·19	43·02	41·21	40·08	
		59·92	58·79	56·98	54·81	52·49	50·14	47·82	45·64	43·70	42·20	41·34	
		62·31	60·47	58·00	55·41	52·84	50·36	48·01	45·83	43·96	42·53	41·74	
		66·53	61·78	59·16	55·98	53·11	50·47	48·00	45·74	43·76	42·23	41·36	

TABLE 2. Pore pressures for the unsymmetric flow configuration shown in figure 5: (*a*) averaged over 100 runs for the uniform-conductance p.d.f.; (*b*) computed via EMT

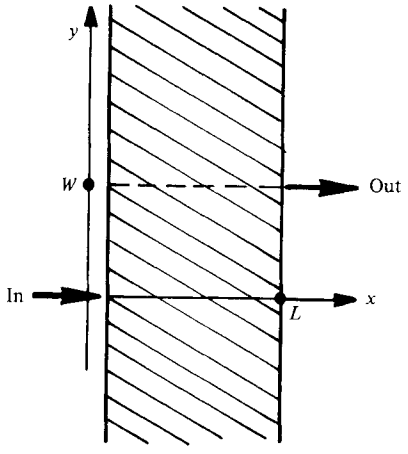

FIGURE 16. An electrical analogy to the flow problem of figure 15.

work as well as they do despite incompetent construction). More generally, in a lattice with $N_\perp \ll N_\parallel$, we find little variation of K with exit pore position until the vertical displacement relative to the entry is 2–3 times $N_\parallel$. In contrast, as the exit pore shifts, the internal pressure field changes greatly, roughly speaking because the average pressure gradient continuously changes direction to be along the line joining entry and exit. As this happens, the distance between entry and exit increases, so the '∇p lines' (analogous to electric field lines) spread out to maintain a constant network conductance.

We can illuminate the above behaviour somewhat by considering a continuum electrical analogy: consider an infinite conducting strip with current I inserted in a

localized region along one boundary and extracted from an adjustable localized region on the other boundary. (See figure 16.) One seeks an electrostatic potential $\phi(\mathbf{x})$ satisfying the Laplace equation

$$\nabla^2\phi = 0$$

in the strip, with boundary conditions on the current density $\mathbf{j} = \alpha\mathbf{E} = -\alpha\nabla\phi$:

$$j_x(0,y) = If(y), \quad j_x(L,y) = If(y-W).$$

Here $f(y)$ is a function localized near $y = 0$ with unit integral. One finds

$$\phi(\mathbf{x}) = \phi(\mathbf{0}) + \frac{I}{4\pi\alpha}\int_{-\infty}^{\infty} \frac{dk\tilde{f}(k)}{k\sinh kL} \times [(e^{iky-kx}-1)(e^{kL}-e^{-ikW}) + (e^{iky+kx}-1)(e^{-kL}-e^{-ikW})],$$

where $\tilde{f}$ is the Fourier transform of f. A convenient choice is

$$f(y) = \frac{1}{\pi}\frac{\epsilon}{\epsilon^2+y^2},$$

for $\epsilon \ll L$, for which the potential difference between entry and exit point is

$$\Delta\phi \simeq \frac{2I}{\alpha}\left[\log\frac{2L}{\epsilon} + \log\cosh\frac{\pi W}{2L}\right].$$

Indeed, the scale of variation of $\Delta\phi$ with W is L, and for sufficiently small ϵ/L the variation is negligible until $W/L \gg 1$.

4.4. *Distribution dependence*

We now study the variation of network conductance with changes in the size distributions of pores and throats. We shall discuss the square lattice in some detail; the others behave in a qualitatively similar manner except that, as EMT predicts, the sensitivity of network conductance to the width of the distribution decreases with σ (cf. table 1). We use the standard flow configuration of figure 9, a square lattice with 10 throats in either direction. It is convenient to consider a 'reference distribution' of pore and throat sizes, with $R = 50\ \mu$m, $r = 25\ \mu$m and $l = 50\ \mu$m, and refer other distributions to it. For this set of values one finds from (27) and (28) a throat conductance of $208\ \mu\text{m}^2$, a pore conductance of $326\ \mu\text{m}^2$, and a centre-to-centre conductance $g_{ab}(\text{reference}) = 91{\cdot}63\ \mu\text{m}^2$. In § 5 we show that, for this lattice g_{ab}, the network conductance, and the Darcy permeability are identical. The selection of the reference and other distributions was made to coincide roughly with the actual dimensions of etched-glass plates now being employed in experimental studies of flow in two-dimensional networks by Chandler (1981).

As remarked at the end of § 2, the pore radius R is numerically irrelevant in W_{aa} and hence in g_{ab}. However, the overall dimensions of the network are determined by the distance between pore centres, from which the throat lengths are given by subtracting two pore radii. The numerical results that follow are stated as a function of the throat-radius and throat-length distributions.

The first issue we address is the effect of shape and width of the distributions about

their mean values. We compare three kinds of distributions of a variable x: delta-function, Gaussian and uniform:

$$\left.\begin{aligned} &\delta(x_0): \quad p(x) = \delta(x - x_0); \\ &G(a,b): \quad p(x) = \frac{c}{\sigma(2\pi)^{\frac{1}{2}}} \exp \frac{(x - \frac{1}{2}(b-a))^2}{2\sigma^2} \quad (x \in [a,b]); \\ &\mathrm{U}(a,b): \quad p(x) = \frac{1}{b-a} \quad (x \in [a,b]). \end{aligned}\right\} \tag{41}$$

Within the second class, we distinguish sharp Gaussian (SG) with $\sigma(b-a)^{-1} = 0{\cdot}1$ and broad Gaussian (BG) with $\sigma(b-a)^{-1} = 0{\cdot}2$. The first set of entries in table 3 compare various broadenings of the reference distribution. The SG distribution is essentially indistinguishable from a delta function, while in the other cases the network conductance decreases with increasing width. This behaviour is understandable from the point of view of EMT, where the averaging in (34) emphasizes the lower part of the conductance p.d.f., as well as from the inequality below (34).

We illustrate the resulting p.d.f.s of network conductances g_{ab} in figure 17 for three cases, corresponding to entries 13, 14 and 15 in table 3. In all cases, the result is a peaked curve skewed towards the lower end. The latter property originates in g_{ab} being, roughly, the square of a symmetrically distributed variable. While the distributions studied here may not correspond precisely to the pore spaces of actual porous media, we do expect realistic conductances to have the general shapes shown in figure 17.

We now compare the conductance of the reference distributions to that of distributions of various average throat radii and lengths. A selection of numerical results is given in the second group of entries in table 3. The general trend of the variation is as expected from (24), (27) and (28): conductance increases roughly quadratically with throat radius, decreases roughly as (const. $+ l)^{-1}$ with throat length, and is independent of pore radius.

We have checked, in a few cases, the EMT conductance against the numerical results in table 3, and found agreement comparable to that in table 1. Going beyond the particular cases studied and approximations in this paper, there are two potential problems for EMT. If the conductance p.d.f., unlike those in figure 17, is heavily weighted near conductance zero (arising, say, from a significant number of very long and narrow throats) the corrections to EMT may be large. In this case, direct numerical solution or the use of critical-point scaling relations (Kirkpatrick 1973) is suggested. A second source of difficulty is the existence of correlations between network elements. If the individual network conductances are not statistically independent the EMT connections are again expected to be larger than we have seen here. There is a formal correlation present in the general expression (24a) for the pore pressures, in that a given pore's radius effects the pressure drop in any of the throats to which it connects. However, in the approximate form (24c), the pore radius drop out and the correlation disappears. In general, the pores will induce some correlation between neighbouring throats and the EMT approximation may not work quite as well.

	$p(r_t)$	$p(l)$	$p(R_p)$	K (μm^2)
1	$\delta(25)$	$\delta(50)$	$\delta(50)$	91·63
2	SG(15, 35)	$\delta(50)$	$\delta(50)$	91·21 ± 0·20
3	BG(20, 30)	$\delta(50)$	$\delta(50)$	90·82 ± 1·75
4	BG(15, 35)	$\delta(50)$	$\delta(50)$	88·67 ± 3·49
5	U(20, 30)	$\delta(50)$	$\delta(50)$	90·13 ± 2·60
6	U(15, 35)	$\delta(50)$	$\delta(50)$	85·69 ± 5·19
7	U(10, 40)	$\delta(50)$	$\delta(50)$	79·05 ± 7·71
8	$\delta(25)$	SG(40, 60)	$\delta(50)$	91·65 ± 0·16
9	$\delta(25)$	SG(30, 70)	$\delta(50)$	91·70 ± 0·33
10	$\delta(25)$	SG(20, 80)	$\delta(50)$	91·79 ± 0·49
11	$\delta(25)$	$\delta(50)$	U(40, 60)	91·63 ± 0·01
12	$\delta(25)$	$\delta(50)$	U(30, 70)	91·61 ± 0·05
13	U(20, 30)	U(40, 60)	$\delta(50)$	89·99 ± 2·48
14	BG(20, 30)	BG(40, 60)	$\delta(50)$	90·83 ± 1·72
15	BG(10, 40)	BG(25, 75)	$\delta(50)$	85·69 ± 5·10
16	$\delta(5)$	$\delta(200)$	$\delta(50)$	0·392
17	U(0·5, 9·5)	$\delta(200)$	$\delta(50)$	0·296 ± 0·059
18	$\delta(12·5)$	$\delta(200)$	$\delta(50)$	5·62
19	U(10, 15)	$\delta(200)$	$\delta(50)$	5·52 ± 0·19
20	U(5, 20)	$\delta(200)$	$\delta(50)$	4·82 ± 0·55
21	U(45, 55)	$\delta(200)$	$\delta(50)$	365·1 ± 5·2
22	U(35, 65)	$\delta(200)$	$\delta(50)$	353·0 ± 15·6
23	$\delta(25)$	$\delta(100)$	$\delta(50)$	63·65
24	$\delta(25)$	U(50, 150)	$\delta(50)$	64·72 ± 1·09
25	$\delta(25)$	U(10, 190)	$\delta(50)$	67·34 ± 2·12
26	$\delta(25)$	U(175, 225)	$\delta(50)$	39·58 ± 0·21
27	$\delta(25)$	U(150, 250)	$\delta(50)$	39·77 ± 0·41
28	$\delta(25)$	U(100, 300)	$\delta(50)$	40·55 ± 0·85

TABLE 3. Network conductance of a 9×10, $\sigma = 4$ lattice for various pore and throat p.d.f.s

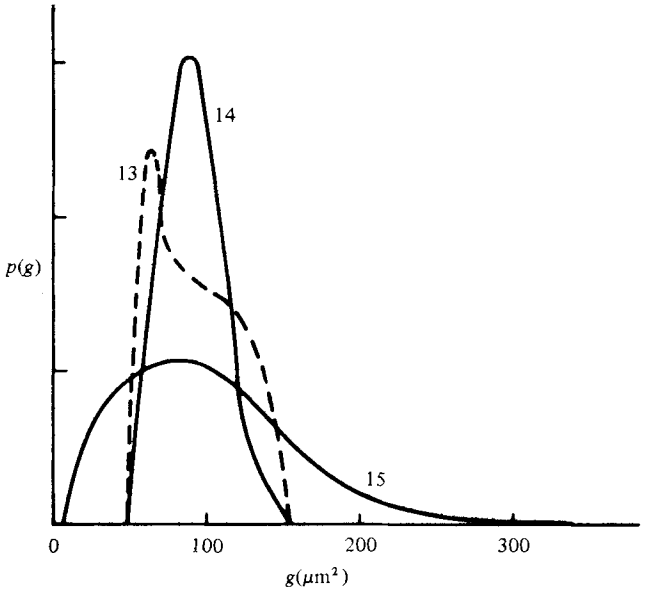

FIGURE 17. Conductance distributions obtained from the throat-size distributions 13–15 in table 3.

5. Permeability

In this section, we use our results on EMT and network conductances to express the Darcy permeability of flow networks in a convenient form. Aside from its being the conventional parameter to describe flow in porous media, the permeability will be seen to have the desirable features, not shared by the network conductance, of being an intensive and rotationally invariant quantity.

We first consider the square lattice with $\sigma = 4$. Once the network has at least several lattice units in each direction, we know from §4 that the random local conductances g_{ab} may be replaced by the EMT average conductance $g_m(4)$. If we apply an external pressure gradient to such a network along one of the lattice axes as in figure 18, then the pattern of fluid flow in the network is as shown in the figure. The total flux and overall pressure difference are

$$Q = N_y q, \quad \Delta p = N_x \frac{q}{g_m(4)},$$

so from (38) the network conductance is

$$K_x(4) = g_m(4) \frac{N_y}{N_x}.$$

In these equations, N_x and N_y are the total number of lattice cells in the x- and y-directions, and we have assumed $N_x, N_y \gg 1$. In all of this section, we deal with lattices satisfying the latter constraint, so that end-effects may be neglected; since the permeability is inherently a macroscopic quantity this is no real limitation. Note also that the details of the pore space are all subsumed into g_m, so figure 18 is a schematic representation of figure 1. The permeability is defined by

$$\mathbf{u} = -k \nabla p, \tag{42}$$

in units where viscosity = 1, and where macroscopic average pressure and velocity are understood. For the uniform flow field in figure 18,

$$|\mathbf{u}| = Q/W, \quad |\nabla p| = \Delta p / L,$$

where W and L are the physical width and length of the network, so that

$$k_x(4) = \frac{Q}{\Delta p} \frac{L}{W} = K_x(4) \frac{L}{W}.$$

For a symmetric square lattice of side l, $L = lN_x$ and $W = lN_y$, so

$$k_x(4) = g_m(4).$$

Unlike K_x, k_x is an intensive quantity, and, as this argument would be identical up to the interchanges $x \leftrightarrow y$ and $L \leftrightarrow W$ if we considered flow in the y-direction, $k_y = k_x$, and the permeability is isotropic as well. Note that we obtain an isotropic permeability because we have assumed that the underlying lattice is statistically isotropic. If the average flow is not along a lattice axis we may decompose it into x- and y-components and use superposition.

For the hexagonal lattice ($\sigma = 3$) of figure 19(a), we proceed similarly. For flow in the x-direction with identical conductances $g_m(3)$, we have the flux pattern shown and

$$Q = N_y q, \quad \Delta p = 2N_x \frac{q}{g_m(3)}.$$

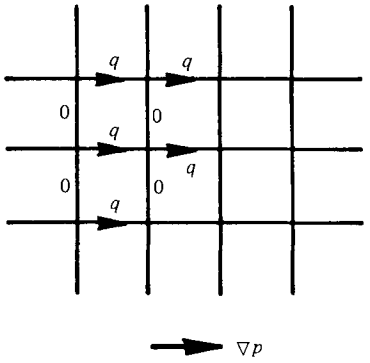

FIGURE 18. Flow patterns in the EMT averaged square lattice.

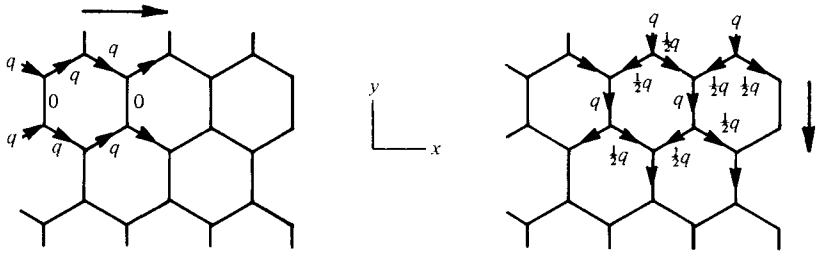

FIGURE 19. Flow patterns in the EMT averaged hexagonal lattice, for two directions of applied pressure gradient.

Here, N_x and N_y are the number of hexagons in the x- and y-directions, and the additional factor of 2 in Δp arises because two links are traversed per hexagon. The lattice length and width are

$$L = 3^{\frac{1}{2}} l N_x, \quad W = \tfrac{3}{2} l N_y,$$

where l is the length of a side, and hence

$$K_x(3) = \tfrac{1}{2} g_{\mathrm{m}}(3) \frac{N_y}{N_x}, \quad k_x(3) = (\tfrac{1}{3})^{\frac{1}{2}} g_{\mathrm{m}}(3).$$

For flow in the y-direction, the pattern of flux is shown in figure 19 (b), for which now

$$Q = N_x q, \quad \Delta p = \tfrac{3}{2} N_y \frac{q}{g_{\mathrm{m}}(3)}.$$

(In this case, three links are traversed for every two hexagons.) L and W are now interchanged from their previous values, and we find

$$K_y(3) = \tfrac{2}{3} g_{\mathrm{m}}(3) \frac{N_x}{N_y}, \quad k_y(3) = (\tfrac{1}{3})^{\frac{1}{2}} g_{\mathrm{m}}(3).$$

As advertised, the permeability is intensive and isotropic.

Identical reasoning applies to each of the two-dimensional lattices L shown in figure 10, and in all cases we find the permeability to be given by

$$k_2(L) = g_{\mathrm{m}}(\sigma) t_2(L) \quad \text{(two-dimensional)}, \tag{43}$$

Lattice	$t_2(L)$	$\phi_2(L)/\phi_2(\text{sq.})$
Hexagonal	$\sqrt{\frac{1}{3}}$	$\sqrt{\frac{1}{3}}$
Kagomé	$\sqrt{\frac{3}{2}}$	$\sqrt{\frac{3}{2}}$
Square	1	1
Trigonal	$\sqrt{3}$	$\sqrt{3}$
Crossed square	3	$1+\sqrt{2} \simeq 2{\cdot}41$

TABLE 4. Geometrical weights and relative porosity (without distinct pores) for two-dimensional networks

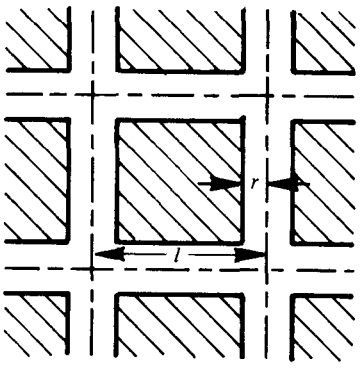

FIGURE 20. The pore space in the absence of distinct pores.

where the numerical factor $t_2(L)$, of geometrical origin, has the values shown in table 4. As above, the permeability is isotropic if the lattice is.†

The geometrical weighting factor $t_2(L)$ is closely related to the porosity of the network, the ratio of void space to total area. The relationship is especially close in one limiting case: suppose the pore space consists entirely of narrow straight channels without district pores, as in figure 10 for the square-lattice case. If the average channel radius is $r \ll l$, the porosity is given by

$$\phi_2(\text{square}) = 4\frac{r(l-2r)}{l^2} \simeq \frac{4r}{l} \quad \text{(no pores)}.$$

Repeating this calculation for the other two-dimensional lattices studied, we find the third column in table 4. To good accuracy (perhaps excepting the crossed-square lattice which is not quite two-dimensional anyway), we find

$$t_2(L) \simeq \phi_2(L)/\phi_2(\text{square}) \quad \text{(no pores)}. \tag{44}$$

In general, with distinct pores present, the correspondence is not so close, but the increase in $t_2(L)$ found upon descending table 4 will be paralleled by an increase in porosity.

For three-dimensional lattices the same reasoning applies. The effect of random network size parameters is to produce random pore-to-pore conductances, which may

† The electrical analogy in (30) can be reversed, and (43) may be regarded as giving the continuum electrical conductivity k of a macroscopic regular network in terms of the EMT electrical conductance of the network elements.

Lattice	σ	$t_3(L)$	$\phi_3(L)/\phi_3(\mathrm{SC})$
Diamond	4	$\frac{1}{4}\sqrt{3}$	$\frac{1}{4}\sqrt{3}$
Simple cubic	6	1	1
Body-centred cubic	8	$\sqrt{3}$	$\sqrt{3}$
Face-centred cubic	12	$2\sqrt{2}$	$2\sqrt{2}$
Hexagonal close-packed	12	$2\sqrt{2}$	$2\sqrt{2}$
Filled body-centred cubic†	16	$\frac{3}{2}\sqrt{3} \simeq 2{\cdot}60$	$\frac{3}{4}+\sqrt{3} \simeq 2{\cdot}48$

† This refers to a lattice formed by superposing simple and body-centred cubic, or including the cube axes in the body-centred structure.

TABLE 5. Geometrical weights and porosity (without distinct pores) for three-dimensional networks

be replaced by an EMT average conductance $g_{\mathrm{m}}(\sigma)$. While we have checked this statement explicitly only for the cubic lattice, one generally expects mean-field approximations such as EMT to perform better in higher spatial dimension (Domb & Green 1976; Koplik 1981). Note that, if the lattice includes distinct pores, the three-dimensional analogue of the calculation in § 2 is required. Once $g_{\mathrm{m}}(\sigma)$ is known, the permeability follows by simple geometric reasoning as above. For example, for a cubic lattice with flow in the x-direction we have

$$Q = qN_yN_z, \quad \Delta p = N_x\frac{q}{g_{\mathrm{m}}(6)}.$$

The lattice length is $L = N_x l$, while instead of the width we consider the cross-sectional area $A = N_yN_zl^2$. The permeability is

$$k\,(\mathrm{cubic}) = \frac{Q}{A}\left(\frac{\Delta p}{L}\right)^{-1} = g_{\mathrm{m}}(6)/l.$$

The factor l, the unit cell size, appears because a three-dimensional fluid conductance has dimension (length)^3 while, in two or three dimensions, permeability has dimension (length)^2. We have evaluated k for several other lattices, obtaining

$$k(L) = g_{\mathrm{m}}(\sigma)t_3(L)/l \quad \text{(three-dimensional)}, \tag{45}$$

where t_3 is given in table 5 and l is the nearest-neighbour separation. Once again, the variation of $t_3(L)$ with lattice is related to variation in porosity: for lattices without distinct pores the porosity $\phi_3(L)$ is given in the third column of table 5. The correlation between t_3 and ϕ_3 is just as close as that between t_2 and ϕ_2, with the only discrepancy occurring for an irregular lattice.

Suppose that instead of a semi-regular network, where the pore centres lie on a regular lattice, we had considered a truly random model porous medium. We would then have to consider a distribution of centre-to-centre distances and co-ordination numbers, but we have seen in § 4.2 that these features are reasonably well accounted for by EMT. We might also consider a number of different possible pore and throat shapes; but these again would be handled by effective-medium averaging. The essential requirement for the applicability of the methods of this paper is the 'factorization' of the porous medium into discrete elements for which the pressure drop is proportional to the fluid flux with a known (geometrical) coefficient.

Since $g_m(\sigma)$ is a relatively slowly varying function of σ (roughly logarithmic, cf. table 1), most of the lattice-to-lattice variation of $k(L)$ will arise from $t(L)$. If we attempt to compare the permeabilities of various real porous media, in general there will be differences both in the lattice used to represent the topology and in the microsopic size distributions of the individual lattice elements. To the extent that the latter are the same, we conclude that permeability is roughly proportional to $t(L)$, and hence to porosity. More generally, we see from (24), (27) and (28) that $g_m \propto D^2$, where D is some characteristic microscopic size parameter of the porous medium, so an approximate form of (43) is

$$k \propto D^2 \phi. \tag{46}$$

Relations of this form are of long-standing use in the petroleum industry to describe the permeability of oil reservoirs (Leverett 1938). While the loose argument just presented is not a derivation, (46) is quite consistent with the ideas in this paper.

In some older approaches to the permeability of porous media, one thinks of the pore space as composed of winding channels of some suitable average radius. One then has Poiseuille flow locally, and the permeability differs from that of a simple straight tube by a 'tortuosity' factor, representing the additional path length induced by the winding (for a review see Scheidegger 1974). In our equations (43) and (45), considering $t(L)$ to represent the porosity, the analogue of tortuosity is the variation of $g_m(\sigma)$ with lattice. However, $g_m(\sigma)$ is a monotonically increasing function of σ, while there is no evident correlation between the tortuousness of flow paths and σ in the lattices shown in figure 10. We feel that the concept of tortuosity is relevant only to media with locally one-dimensional flow paths, and is not an appropriate description of flow in interconnected networks.

6. Conclusions

We have discussed creeping flow in a class of semi-regular network models of porous media. The principal new features of this work are as follows.

(i) The inclusion of pores, or junctions between flow channels, in a network formalism. Previous network studies of this type have considered only collections of straight tubes.

(ii) The applicability and utility of effective-medium theory has been stressed. The randomness in the flow-network elements may be averaged over in an almost analytic fashion. The validity of Darcy's law for even relatively small samples of materials with a strongly varying microscopic geometry follows from EMT.

(iii) We have expressed the permeability of flow networks in a convenient explicit form (43), (45). For any network, k is given as a factor depending on the local topology and the microscopic size distribution and a factor depending on the global network topology.

Several further related problems are suggested by the present work. By using numerical techniques one can improve upon the approximations made in the pore-flow calculation of § 2, and extend the calculations to pores of a less convenient shape and to pores in three dimensions. It would also be worth while to verify the EMT approximation explicitly for truly random networks. While we have only treated networks that are statistically homogeneous and isotropic, many interesting porous media are not. It is quite straightforward to study inhomogeneity and anisotropy numerically,

but the appropriate modifications of EMT ideas are not known. A further interesting extension is to the flow of several immiscible fluids in a porous medium. Here one must deal with capillary forces and time-dependent flows, but to the extent that one can employ a Washburn approximation (Washburn 1921; Dussan V. 1979), the problem can still be formulated in linear-network form. We hope to report on some of these matters soon.

I thank G. K. Batchelor, R. N. Chandler and E. J. Hinch for discussions, and K. Kaplin and T. J. Lasseter for assistance with the numerical computations.

REFERENCES

BALIAN, R., MAYNARD, R. & TOULOUSE, G. (eds) 1979 *Ill-Condensed Matter*. North-Holland.

BEAR, J. 1972 *Dynamics of Fluids in Porous Media*. Elsevier.

CHANDLER, R. N. 1981 To be published.

COLLINS, R. E. 1961 *Flow of Fluids Through Porous Material*. Reinhold.

DOMB, C. & GREEN, M. S. (eds) 1976 *Phase Transitions and Critical Phenomena*, vol. 6. Academic.

DULLIEN, F. A. L. 1979 *Porous Media: Fluid Transport and Pore Structure*. Academic.

DUSSAN V., E. B. 1979 *Ann. Rev. Fluid Mech.* **11**, 371.

FATT, I. 1956 *Trans. A.I.M.E.* **207**, 160.

KANTOROVICH, L. V. & KRYLOV, V. I. 1958 *Approximate Methods of Higher Analysis*. Noordhoff.

KIRKPATRICK, S. 1973 *Rev. Mod. Phys.* **45**, 574.

KOPLIK, J. 1981 *J. Phys.* C: *Solid State Phys.* **14**, 4821.

LEVERETT, M. C. 1938 *Petrol. Technol.* **1**, 1.

MILLS, R. D. 1977 *J. Fluid Mech.* **79**, 609.

MOFFATT, H. K. 1964 *J. Fluid Mech.* **18**, 1.

MUSKHELISHVILI, N. I. 1953 *Some Fundamental Problems in the Mathematical Theory of Elasticity*. Noordhoff.

PRATT, W. K. 1978 *Digital Image Processing*. Wiley.

PIRSON, S. J. 1963 *Handbook of Well-log Analysis*. Prentice-Hall.

SCHEIDEGGER, A. E. 1974 *The Physics of Flow in Porous Media*, 3rd edn. University of Toronto Press.

SERRA, J. 1982 *Image Analysis and Mathematical Morphology*. Academic.

VAN BRAKEL, J. 1975 *Powder Technol.* **11**, 205.

WASHBURN, E. W. 1921 *Phys. Rev.* **17**, 273.

ZIMAN, J. M. 1979 *Models of Disorder*. Cambridge University Press.